27.2 An Adiabatic Sense and Set Rectifier for Improved Maximum-Power-Point Tracking in Piezoelectric Harvesting with 541% Energy Extraction Gain

Yimai Peng, David Kyojin Choo, Sechang Oh, Inhee Lee, Taekwang Jang, Yejoong Kim, Jongyup Lim, David Blaauw, Dennis Sylvester

University of Michigan, Ann Arbor, MI

Piezoelectric energy harvesters (PEHs) convert mechanical energy from vibrations into electrical energy. They have become popular in energy-autonomous IoT systems. However, the total energy extracted by a PEH is highly sensitive to matching between the PEH impedance and the energy extraction circuit. Prior solutions include the use of a full-bridge rectifier (FBR) and a so-called synchronous electric-charge extraction (SECE) [1], and are suitable for non-periodic vibrations. However, their extraction efficiency is low since the large internal capacitance C_p (usually 10's of nF) of the PEH (Fig. 27.2.1) prevents the output voltage from reaching its maximum power point (MPP) under a typical sinusoidal and transient excitation ($V_{MPP} = ½·I_pR_p$). A recently proposed technique [2,3,4], called bias-flip, achieves a higher extraction efficiency by forcing a predetermined constant voltage at the PEH output, V_p, which is then flipped every half-period of the assumed sinusoidal excitation (Fig. 27.2.1, top left). To flip V_p, the energy in capacitor C_p is extracted using either a large external inductor [2,3] or capacitor arrays [4]. It is then restored with the opposite polarity (Fig. 27.2.1, top). However, V_{MPP} of the PEH varies with sinusoidal current I_p; hence, the two fixed values of V_p in the flip-bias technique either over- or underestimate V_{MPP} for much of the oscillation cycle (pattern filled regions in Fig. 27.2.1, top right). In addition, none of the prior approaches compensate for V_{MPP}-waveform amplitude changes, due to input intensity variations or decaying oscillations after an impulse, further degrading efficiency.

This paper proposes a sense-and-set (SaS) MPP-tracking interface circuit that extracts near-optimal power from the PEH. The SaS circuit dynamically measures V_{MPP} and sets the PEH output voltage (V_p) to match and follow the V_{MPP} waveform (step A, Fig. 27.2.1 bottom). After adjusting V_p to V_{MPP}, all switches are turned off and I_p naturally charges C_p (step B), achieving near-optimal extraction efficiency. The circuit harvests energy from C_p after a short, pre-determined time ($t_{A.1}$) to maintain V_p near V_{MPP} (step C). To reduce energy overhead, SaS performs all operations adiabatically using only a single external inductor and capacitor. Since SaS does not presume any particular PEH current waveform, it applies to both periodic and non-periodic use cases. SaS was implemented in 180nm CMOS and achieves a 5.41× power-extraction improvement (FOM) for periodic excitations and a 4.59× improvement for shock excitations compared to an ideal FBR.

The key challenge for efficient harvesting is repeatedly determining V_{MPP} that changes with the PEH current variation, with low overhead. SaS performs a series of steps (A.1–A.4, Fig. 27.22) that measure I_p and convert it to a voltage V_T on capacitor C_T, which becomes a reference for charging or discharging V_p to reach V_{MPP}. Initially in step A.1, S7 and S5 are closed and C_p and C_p' are charged to equal potentials. Then, S7 is opened for a brief time ($t_{A.1}$ ≈100µs) and I_p only charges C_p. Since I_p determines V_{MPP}, and observing that I_{Rp} can be approximated as constant during $t_{A.1}$, V_{MPP} is derived from the resulting voltage difference ΔV between C_p and C_p', as expressed by Eq. 1 shown in Fig. 27.2.2. Usually ΔV is very small (~1mV), since C_p is large and it is desirable to keep $t_{A.1}$ short, hence it is challenging to resolve using a conventional comparator or ADC. However, the stored energy difference between C_p and C_p' is relatively large (~pJ), thus we propose using a charge-based amplifier to transfer this energy difference into a small capacitor (C_T) using the inductor (L) in step A.3, thereby obtaining a much higher voltage V_T. In the absence of parasitics we obtain $V_{MPP} = ½·(V_T + V_1)$ (a variation of Eq. 3 in Fig. 27.2.2) by appropriately sizing $C_T = ½·C_p·(t_{A.1}/R_pC_p)^2$. After we have generated V_{MPP} from V_T and V_1 (as shown in Fig. 27.2.3) we adjust V_p in step A.4 to V_{MPP} adiabatically using the same inductor.

Figure 27.2.3 shows the circuit details for SaS. All switches are implemented using transmission gates and are controlled using a pre-configured sequence of pulses. A 5-stage ring oscillator and pulse generator produce the correct pulse length and sequence. Both of these employ leakage-based invertor cells [5] to ensure high energy-efficiency across a very wide frequency range (10-100kHz). Two clocked comparators further modulate (truncate) critical pulses that operate at a faster frequency (5MHz). Optimally sized drivers then buffer the pulses to generate the final switch-control signals. To generate $V_{MPP} = ½·(V_T + V_1)$ (Eq. 3 in Fig. 27.2.2), V_1 is sampled by capacitor C_{V1} (same size as C_T) and shorted to C_T. However, the off-chip inductor L introduces significant parasitics to ground, reducing the value of V_T. We compensate for this using the series-parallel structure (Fig. 27.2.3) and adjusting C_{V1} appropriately to generate $V_{MPP} = ½·n·(V_T + V_1)$, where n can be tuned between 1-5. Comparator CMP_1 then compares PEH output V_p with the generated V_{MPP} to set $V_p = V_{MPP}$ (Fig. 27.2.3, red path). Once V_p arrives at the correct value, a recycling path for the remaining energy in L is turned on until the second comparator CMP_2 detects the zero-crossing point of the inductor current necessary for adiabatic operation (Fig. 27.2.3, green path).

The value of C_p varies across the PEH type; hence, for each new PEH C_T must adjusted. We enable this by first choosing an appropriate C_T from an on-chip capacitor array (0.2–9.2pF with 0.2pF steps, omitted from Fig. 27.2.3 for clarity), followed by tuning the duration of step A.1 ($t_{A.1}$). The proposed harvester automatically performs this tuning by running through steps A.1–A.4 using a modified operation of the series-parallel capacitor structure such that V_p is set to V_{oc} ($2·V_{MPP}$) instead of V_{MPP}. Then, an additional sensing step A.1–A.3 is applied and the polarity of V_T is determined. If $t_{A.1}$ is tuned correctly and V_p is set at V_{oc}, then $\Delta V = 0$ at the end of step A.1; therefore, $V_T = 0$ after step A.3. By repeating this process while sweeping the value of $t_{A.1}$ and observing the change in sign of V_T, SaS automatically finds the point where $\Delta V = 0$ and $t_{A.1}$ is correctly tuned.

When I_p changes polarity so does V_{MPP}, which results in additional operating complexity for both a positive and negative V_{MPP}. Instead, SaS detects the I_p sign change by comparing V_{MPP} against ground with comparator CMP_1 (for simplicity switches that connect ground to the comparator'sinverse input are not shown in Fig. 27.2.3). SaS then performs two additional steps: (1) it extracts the remaining energy from C_p into L, and (2) it flips the two terminals of the PEH (flip switch in Fig. 27.2.3) and restores the extracted energy. It then proceeds as before, tracking a positive V_{MPP}. As a result, no negative voltages, thus simplifying harvester design.

The proposed SaS circuit is fabricated in 180nm CMOS and occupies 0.47mm^2. It is tested with a commercial PEH (Mide PPA-1022) on a shaker table (Unholtz-Dickie model 650) with a 10.6g tip mass. Figure 27.2.4 shows the measured MPPT-operation waveform for both periodic (85Hz) and shock excitations (1 pulse/s). During the start-up phase the maximum value of V_P is limited by V_{out}. As V_{out} builds the efficiency of the SaS circuit gradually increases and eventually tracks the MPP. After start-up the SaS circuit first auto-calibrates to adapt to the specific PEH parasitics (C_p and R_p) by tuning $t_{A.1}$. Following calibration, V_p dynamically adjusts to various PEH input characteristics across different excitation types and amplitudes, including weak amplitudes that are typically difficult to track (Fig. 27.2.4, weak periodic). Due to voltage limitations of our CMOS process, V_p is limited to 2V, even though the MPP voltage reaches higher than that for strong amplitudes (Fig. 27.2.4 strong periodic and shock input). An external voltage supply is used for accurate measurement of the SaS circuits' power overhead. Measured leakage and active power for the SaS circuit under a 2V-supply voltage are 7nW and 230nW.

Figure 27.2.5 (top) shows SaS measured output power across different output voltages (V_{OUT}) and different excitation levels. As long as $V_{OUT} < V_{MPP}$ the SaS circuit can perform true MPPT and extract the maximum power available. For stronger excitations ($V_{MPP} > V_{OUT}$) SaS operates off-MPPT due to the aforementioned CMOS voltage limit, but still harvests energy at a higher efficiency than a conventional FBR or a bias-flip circuit. Note that the circuit could be reconfigured in step A.4 to serve as a boost converter (requiring an additional switch configuration), or implemented with a high voltage process to extend the voltage range. Figure 27.2.5 (bottom left) shows the measured output power using different MPP tracking frequencies. Higher tracking frequencies allow SaS to adjust V_p more frequently and track V_{MPP} more accurately, improving harvesting efficiency, but this also leads to larger losses during energy transfer: due to both conduction and switching losses. The optimal frequency was found to be 2.5kHz for a 85Hz excitation.

Measurements show a 5.41 and 5.56× power extraction improvement (FoM) compared to an ideal FBR with strong and weak periodic excitation input. Shock excitation improvement is calculated to be 4.59×. Since the FoM depends on the PEH Q value (ωR_pC_p), we also report the improvement normalized to Q in Fig. 27.2.6. The proposed SaS circuit achieves nearly 2× energy extraction improvement, based on a Q-normalized FoM, compared to prior-art. It also offers the unique and practical ability to adapt to different excitation types and levels dynamically.

Acknowledgments:
The authors would like to thank Robert Gordenker and Professor Khalil Najafi at the University of Michigan, for their support and contribution to this project.

References:

[1] A. Quelen, et al., "A 30nA Quiescent 80nW-to-14mW Power-range Shock-optimized SECE-based Piezoelectric Harvesting Interface with 420% Harvested-energy Improvement," *ISSCC*, pp. 120-121, 2018.

[2] Y.K. Ramadass, et al., "An Efficient Piezoelectric Energy Harvesting Interface Circuit Using a Bias-Flip Rectifier and Shared Inductor," *JSSC*, vol. 45, no. 1, pp. 189-204, Jan. 2010.

[3] S. Du, et al., "A fully integrated split-electrode synchronized-switch-harvesting-on-capacitors (SE-SSHC) rectifier for piezoelectric energy harvesting with between 358% and 821% power-extraction enhancement," *ISSCC*, pp. 152-154, 2018.

[4] Z. Chen, et al., "A 1.7mm^2 Inductorless Fully Integrated Flipping-capacitor Rectifier (FCR) for Piezoelectric Energy Harvesting with 483% Power-extraction Enhancement," *ISSCC*, pp. 372-373, 2016.

[5] I. Lee, et al., "A Constant Energy-Per-Cycle Ring Oscillator Over a Wide Frequency Range for Wireless Sensor Nodes," *JSSC*, vol. 51, no. 3, pp. 697-711, Mar. 2016.

 978-1-5386-8531-0/19/$31.00

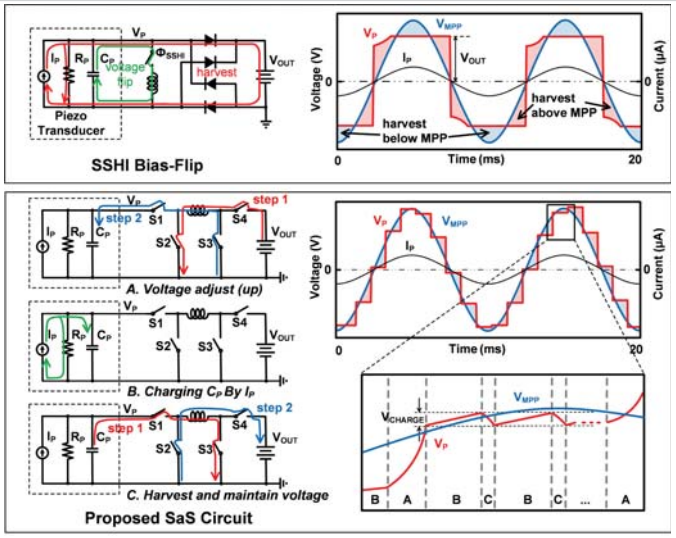

Figure 27.2.1: Circuit diagram and operation waveform for PEHs with SSHI (bias-flip) technique and proposed SaS circuit.

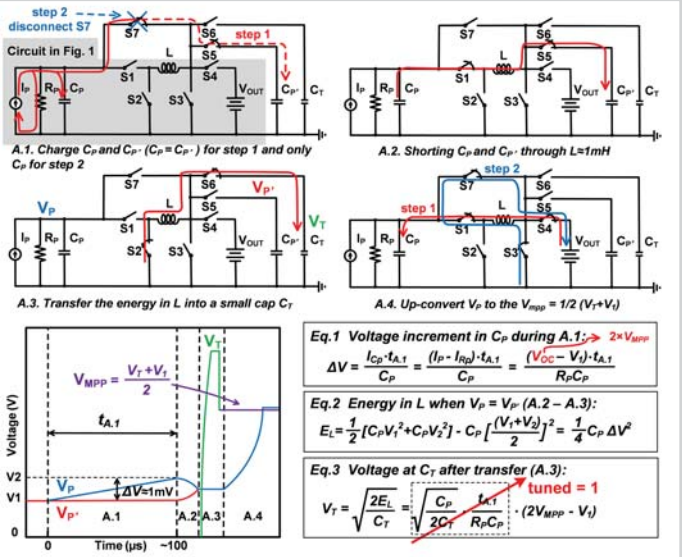

Figure 27.2.2: SaS operation sequences/waveforms for MPP-tracking.

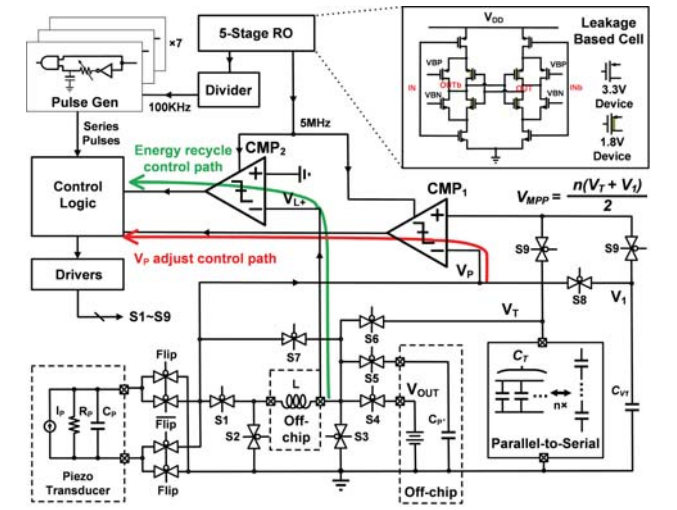

Figure 27.2.3: Proposed SaS circuit details: Inductor-sharing switches, leakage-based low power clock/timing circuit and clocked-comparator circuit for switch control.

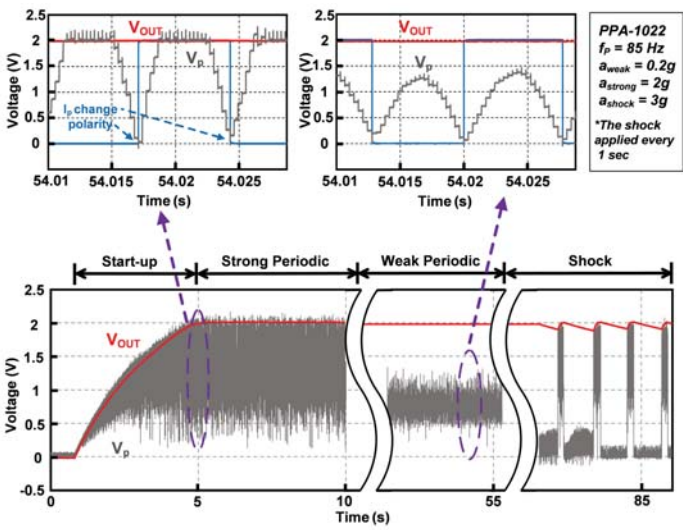

Figure 27.2.4: Measured waveform of MPPT process for strong periodic, weak periodic and shock excitation by the proposed SaS circuit.

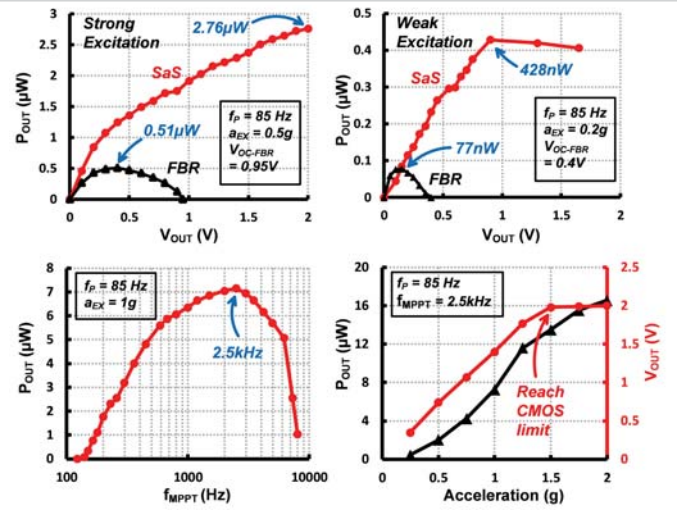

Figure 27.2.5: Measured SaS harvested power with different excitation types, acceleration levels and MPP tracking frequency, compared to a full-bridge rectifier.

References	This Work		ISSCC'18[1]	JSSC'10[2]	ISSCC'16[3]	ISSCC'18[4]
Technology	0.18 μm		40 nm	0.35 μm	0.35 μm	0.18 μm
Energy Extract Technique	SaS		SECE	SSHI	SSHI	SSHC
Technique's Key Component	L = 1 mH $C_{P'}$ = 10 nF		L = 2.2 mH	L = 0.82 mH	L (value not reported)	C_{flip} = 8× C_p
PEH Type	MIDE PPA-1022		MIDE PPA-1011	MIDE V22B	MIDE V21B & V22B	CUSTOM MEMS
C_p	8 nF		43 nF	9 nF	9 – 26 nF	1.94 nF
Frequency	85 Hz		75.4 Hz	225 Hz	134.6 - 229.2 Hz	219 Hz
Excitation Type	Periodic & Shock		Periodic & Shock	Periodic	Periodic & Shock	Periodic
FoM [a] (Periodic)	(strong) **5.41×**	(weak) **5.56×**	3.14×	4×	4.40×	8.21×
FoM / Q_{PEH} [b] (Periodic)	**0.316**	**0.325**	0.132	0.168	0.119	Unknown
PEH V_{OC} for Reported FoM	**0.95 V**	**0.4 V**	2.85 V	2.4 V	0.95 V	2.5 V
FoM (Shock)	**4.59×**		4.20×	N/A	2.69×	N/A
Auto-maintain MPPT [c]	**Yes**		No	No	No	No

(a) $FoM = \frac{\max(P_{out})}{\max(P_{FBR})}$, which for periodic excitation can also be calculated by $\frac{\max(P_{out})}{C_p f_p V_{oc}^2}$

(b) Q_{PEH} is measured for this work and calculated for prior arts, according to the reported PEH type and frequency;

(c) SECE and Bias-Flip need to lower V_{OUT} for smaller excitations to maintain MPPT, while SaS does not require this.

Figure 27.2.6: Measured performance and comparison table to prior-art.

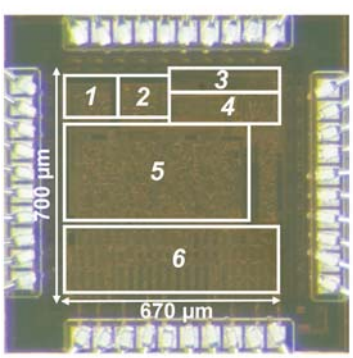

1 Bias voltage generator
2 Clock generator
3 Scan chain for tuning control
4 Comparators and control logic
5 Pulse generator
6 SaS switches

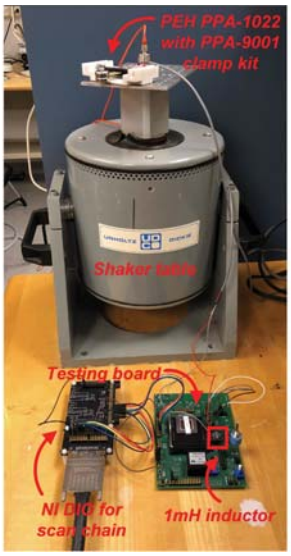

Figure 27.2.7: Die photograph and testing setup.

978-1-5386-8531-0/19/$31.00